1 **TITLE:**

2 Underground Coal Gasification – A numerical approach to study the formation of syngas and its reactive transport

3 in the surrounding strata

4

5 Author 1

6 ● Renato Zagoršćak, PhD, MSc, BSc; Research Associate

7 ● Geoenvironmental Research Centre (GRC), Cardiff School of Engineering, Cardiff University, Cardiff,

8 Wales, UK

9 Author 2

10 ● Ni An, PhD, MSc, BSc; Research Associate (Corresponding author: Ann@cardiff.ac.uk)

11 ● Geoenvironmental Research Centre (GRC), Cardiff School of Engineering, Cardiff University, Cardiff,

12 Wales, UK

13 Author 3

14 ● Rupesh Palange; PhD Student; Research scholar

15 ● Department of Mechanical and Industrial Engineering, Indian Institute of Technology Roorkee, Roorkee,

16 India

17 Author 4

18 ● Michael Green, PhD

19 ● UCG Engineering Ltd, UK, Founding Director

20 ● Surbiton, Surrey KT6 6QB, United Kingdom

21 Author 5

22 ● Murugesan Krishnan, PhD, M.Tech, B.E.; Professor

23 ● Department of Mechanical and Industrial Engineering, Indian Institute of Technology Roorkee, Roorkee,

24 India

25 Author 6

26 ● Hywel Rhys Thomas, BSc, MSc, DIC, PhD, DSc, ACIPR, CEng, FGS, FREng, FRS, FLSW, MAE; Professor

27 and Director

28 ● Geoenvironmental Research Centre (GRC), Cardiff School of Engineering, Cardiff University, Cardiff,

29 Wales, UK

30
31

32 **Full contact details of corresponding author.**

33 **Dr Ni An**

34 **Geoenvironmental Research Centre (GRC), Cardiff School of Engineering, Cardiff University**

35 **Queen's Buildings, The Parade, Cardiff CF24 3AA, Wales, UK**

36 **+44(0)29 2078 6264**

37

38   **Abstract**

39   In this work, a method to study the formation of syngas during the underground coal gasification (UCG) process

40   and its reactive transport in the surrounding strata is proposed. It combines a thermodynamic equilibrium

41   stoichiometric model of the cavity reactions with a coupled thermo-hydraulic-chemical-mechanical (THCM)

42   framework of COMPASS code for the transport of UCG products away from the cavity. With the input

43   information of coal properties obtained from the South Wales coalfield, gasification reagents (air and steam) and

44   thermodynamic conditions (initial temperature and pressure), the thermodynamic equilibrium model developed

45   provides the maximum yield of gasification products and temperature from a UCG system. Gasification results

46   giving the syngas composition with the highest percentage of methane and carbon dioxide, are then used as the

47   chemical (gas) and thermal boundary conditions for the coupled thermo-chemical model of the THCM framework

48   to analyse the variations of temperature and gas concentrations, in strata surrounding the UCG reactor. For that

49   purpose, a set of numerical simulations considering three porous media (coal, shale and sandstone) with different

50   physico-chemical properties is conducted. The gasification results demonstrate that increasing the amount of

51   steam injected in the UCG reactor decreases the temperature of the system as well as the concentration of carbon

52   monoxide and nitrogen, while benefiting the production of hydrogen, methane and carbon dioxide. The numerical

53   simulations performed using the THCM model indicate that multicomponent gas diffusion and advection are

54   competing transport mechanisms in porous media with intrinsic permeability higher than 1 mD (sandstone), while

55   the gas diffusion becomes a dominant transport process in porous media with an intrinsic permeability lower than

56   1 mD (coal and shale). Moreover, the simulation results of reactive transport of methane and carbon dioxide in

57   different porous media demonstrate the significance of considering the adsorption effect in the gas transport in

58   the overall UCG process. In particular, the retardation of the gas front due to gas sorption is the most pronounced

59   in coal, followed by shale and then sandstone. In conclusion, the model presented in this study demonstrates its

60   potential application in managing the environmental practices, reducing pollution risk and securing greater public

61   and regulatory support for UCG technology.

62

63   **Keywords**:

64   Energy; Underground coal gasification; Equilibrium model; Coupled modelling; Gas flow; Sorption

65

1. Introduction

Coal reserves significantly exceed those of oil and gas, however less than one-sixth of the world's coal is currently economically accessible using conventional mining methods [1]. Underground coal gasification (UCG) is a process whereby coal deposits that are either too deep underground or too costly to be extracted using traditional mining techniques, are converted into a combustible gas, commonly known as syngas. A UCG operation consists of a series of injection and production wells drilled into a coal seam where reactant gases, i.e. air, oxygen or steam, are supplied (Fig. 1). As having a fully instrumented UCG trial with comprehensive data extraction is challenging and expensive, computational modelling offers an inexpensive way for predicting the complex interaction of various processes involved during and beyond the UCG operation.
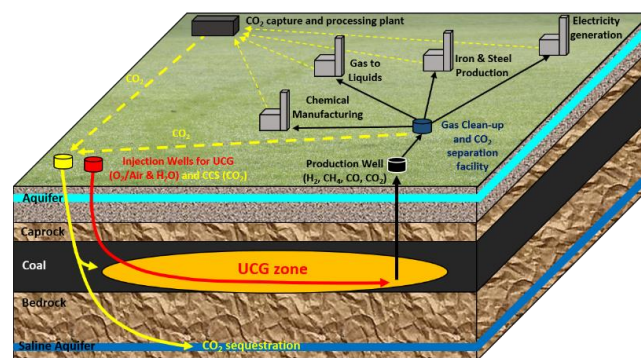
Fig. 1. Schematic diagram of the overall UCG process

An extensive literature review given in Khan et al. [2] and Perkins [3], suggests that current numerical models predominantly focus on the phenomena of coal gasification and cavity formation [3], the product gas compositions and quality [4-6], underlying thermo/mechanical/chemical reactions and heat and mass transport phenomena in the permeable bed and newly formed cavity [7-12]. Those numerical models are then applied to predict the effect of various physical and operating parameters on the performance of the UCG process and provide suggestions for the economic and technical feasibility of UCG technology. For instance, an innovative thermodynamic underground coal gasification model was proposed firstly by Klebingat et al. [12] to optimize the coupled synthesis gas quality and simultaneously reduce tar yields under given geological boundary conditions and then applied further by Klebingat et al. [13] to provide a predictive UCG analysis taking into account tar production control and economic gas quality constraints to achieve optimum operating options in view of synthesis gas quality and reduced tar production. Other models focus on the geo-mechanical phenomena in the surrounding strata dealing with the stress-strain changes as a result of thermo-mechanical induced effects and potential surface subsidence changes [14, 15].

90   Besides primary gas components, i.e. methane, hydrogen, carbon monoxide and carbon dioxide, a number

91   of organic and inorganic contaminants, such as phenols, benzene, sulphates, metal and metalloid elements can be

92   generated and released during the UCG process [16]. The UCG has been performed in over 75 trials throughout

93   the world, and despite most of the UCG trials not experiencing significant environmental issues, potential

94   pollution is the biggest public and regulatory concern [17]. Several researchers who focused on the generation

95   and transport of contaminants via experimental and numerical analyses [18-25] have suggested that operating the

96   UCG process above the hydrostatic pressure can pose an environmental concern due to the chemical reactions in

97   the groundwater environment depending on mineral composition, temperature, concentration of syngas

98   components and the chemical composition of groundwater. However, modelling of contaminant transport and

99   reactions received less attention as it is a complex process with multiple aspects involving heat, mass, stress-strain

100   and physico-chemical reactions [18, 26]. For example, little is known of how the gas sorption affects the gas

101   migration around the UCG cavity and whether it can help to retard potential gas leakage. Upadhye et al. [27]

102   concluded that general hydrogeological models are not appropriate for predictions and assessments related to

103   groundwater pollution and environmental issues in the context of UCG as such models often do not include the

104   complexity of the processes and effects involved in UCG. Therefore, modelling platforms possible to

105   simultaneously simulate the production of syngas, the environmental impact of UCG products both in liquid and

106   gaseous state and the geo-mechanical impacts of the UCG in complex multi-well configurations are therefore

107   required to enhance the understanding of all the environmental aspects related to UCG [3]. Performing such work

108   is also crucial in order to demonstrate to the regulatory bodies and the public under which conditions UCG can be

109   feasible without generating environmental damage and pollution.

110   In this paper, a comprehensive thermodynamic and coupled thermo-hydro-chemical-mechanical (THCM)

111   modelling approach is presented. Through specific process parameters, a thermodynamic equilibrium

112   stoichiometric model for calculating syngas concentrations and reaction temperature has been coupled with the

113   existing THCM framework of the COMPASS software which has a background of high-performance simulations

114   of three-dimensional multiphase, multicomponent reactive transport in porous geomaterials [28-30]. The

115   developed model is then applied to investigate the gas migration and the effect of its sorption on transport through

116   different geological media (coal, shale and sandstone) surrounding the UCG cavity, considering the scenario of

117   potential syngas leakage.

118

119   **2. Theoretical framework**

120   In this section, a theoretical framework is presented consisting of a thermodynamic equilibrium stoichiometric

121   model and a coupled thermo-chemical model contained within the thermo-hydraulic-chemical-mechanical

122   framework of the COMPASS Code (Fig. 2). The thermodynamic equilibrium model has been developed based

123   on the previous work on biomass and coal gasification [31, 32] and is being incorporated within the COMPASS

124   framework through the boundary condition interface, i.e. the results of individual syngas concentrations and the

125   reactor temperature serve as an input for the reactive transport modelling. The COMPASS code is a coupled

126   thermo-hydro-chemical-mechanical model, previously developed at the Geoenvironmental Research Centre by

127   Thomas and co-workers [28-30, 33, 34] to address various geo-environmental issues. COMPASS is based on a

128   theoretical formulation that can be described as a mechanistic approach. The various mechanisms of behaviour

129   are included in an additive manner with inter-related couplings being accommodated. The model is based on mass

130   conservation for moisture, gas and chemical transport and energy equation for the heat transfer. Mechanical

131   behaviour is also included via an appropriate constitutive relationship using the elasto-plastic approach.
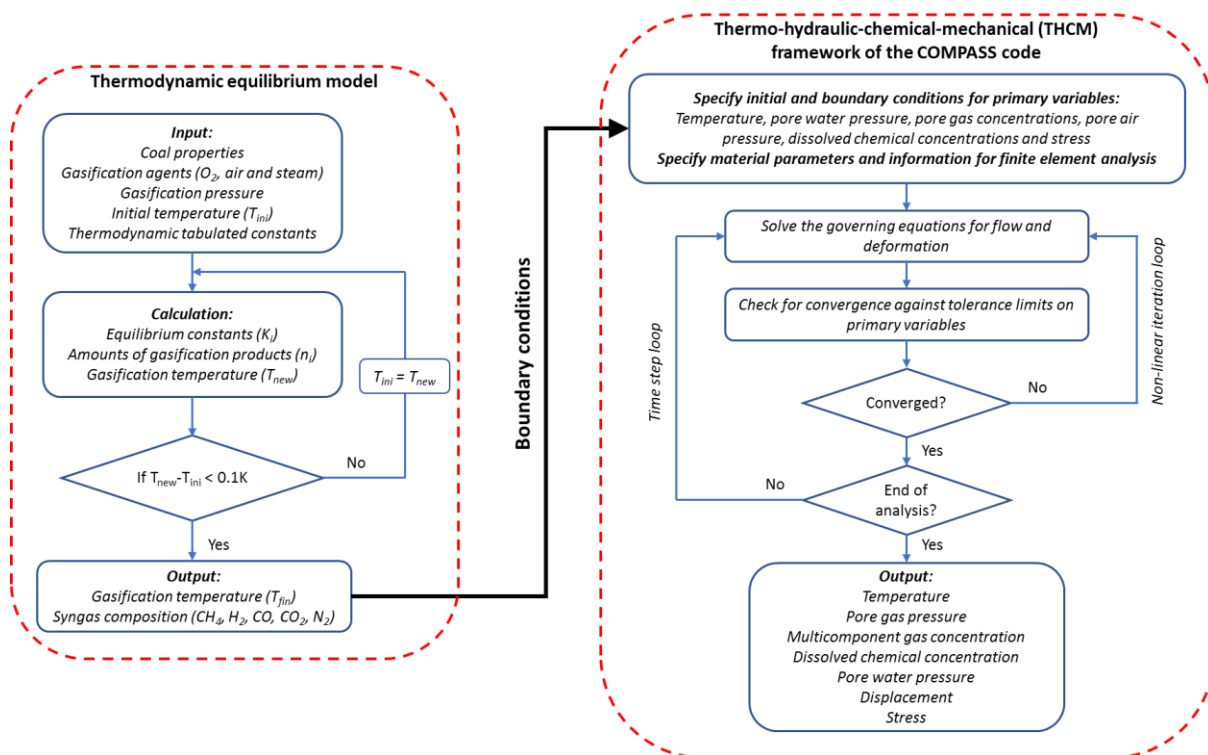
132

133   Fig. 2. Numerical approach consisting of a thermodynamic equilibrium stoichiometric model and a coupled

134   thermo-hydraulic-chemical-mechanical framework of the COMPASS code

135

136   The COMPASS code has been successfully extended by including the advanced geochemical model PHREEQC

137   (version 2) [35]. Through both equilibrium and kinetically controlled geochemical reactions, the model is capable

138   to simulate the reactive transport and fate of multicomponent and dissolved chemicals and gases. The geochemical

139   reactions considered in the coupled model include phase transformation, ion exchange, precipitation and

140   dissolution of minerals, surface complexation and redox reactions. The transport model (COMPASS) and the

141   geochemical model (PHREEQC) are linked together using a sequential non-iterative approach [29]. Further details

142   of the applied models are provided in the following sections.

143

144   **2.1. Thermodynamic model**

145   The production of syngas using gasification is a complex process that depends on several factors including the

146   composition of feedstock, the gasifier conditions, temperature and pressure, and the type and amount of oxidiser

147   and moderator. A thermodynamic equilibrium modelling approach is widely used to evaluate the performance of

148   gasification system in terms of product gas composition and efficiency [31, 32].

149   The global gasification reaction for one mole of feedstock can be represented as:

$$CH_xO_yN_z + m(O_2 + 3.76N_2) + nH_2O + wH_2O \tag{1}$$

$$\rightarrow x_1H_2 + x_2CO + x_3CO_2 + x_4H_2O + x_5CH_4 + \left(^z/_2 + 3.76m\right)N_2$$
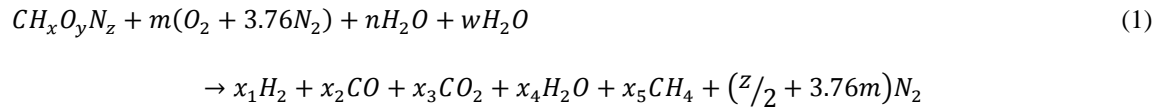
150   where $CH_xO_yN_z$ is the chemical formula for the feedstock/coal, subscripts x, y and z are the number of moles of

151   hydrogen, oxygen, nitrogen in feedstock per mole of carbon, n represents the amount of moisture per mole of

152   feedstock, m represents the amount of air supply per mole of feedstock and w represents the amount of steam

153   supply in mole per mole of feedstock. The coefficients x_1, x_2, x_3, x_4, x_5 represent the number of moles of H_2,

154   CO, CO_2, H_2O and CH_4, respectively. The molar concentrations of syngas products and gasification temperature

155   together comprise of six unknowns and are output data from the model. Hence, six equations are required to

156   determine six unknowns, three of which will be obtained from the mass balance for the global gasification

157   reaction.

158   Carbon balance gives:

$$x_2 + x_3 + x_5 = 1 \tag{2}$$

159   Hydrogen balance gives:

$$2x_1 + 2x_4 + 4x_5 = x + 2n + 2w \tag{3}$$

160   Oxygen balance gives:

$$x_2 + 2x_3 + x_4 = y + 2m + n + w \tag{4}$$

161   To obtain the remaining equations, chemical reactions as an integral part of the gasification process are

162   used. By combining the Boudouard reaction and the water-gas reaction, the water-gas shift reaction can be

163   obtained and is given as [36]:

$$CO + H_2O = CO_2 + H_2 \tag{5}$$

164 Methanation reaction gives:

$$C + 2H_2 = CH_4 \tag{6}$$

165 The equilibrium constant for the water-gas shift reaction is:

$$K_1 = \frac{x_1 x_3}{x_2 x_4} \tag{7}$$

166 The equilibrium constant for the methanation reaction is:

$$K_2 = \frac{x_5}{x_1^2} \left(\frac{P}{x_T P_0} \right)^{-1} \tag{8}$$

167 where x_T is the total sum of all the product gaseous species, P is the pressure and P_0 is the standard reference state

168 pressure.

169   In order to solve the non-linear equations (7) and (8), the values of the reaction constants must be calculated

170 using the following equation:

$$lnK_i = \frac{-\Delta G^0}{RT} \tag{9}$$

171 Where R is the universal gas constant and ΔG^0 is the standard Gibbs function at a given temperature T.

172   The dependence of ΔG^0 on temperature can be expressed through heat of formation which is further

173 expanded in terms of specific constants as [37]:

$$\frac{dlnK}{dT} = \frac{\Delta H^0}{RT^2} \tag{10}$$

$$\frac{\Delta H^0}{R} = \frac{J}{R} + (\Delta A)T + \frac{\Delta B}{2}T^2 + \frac{\Delta C}{3}T^3 - \frac{\Delta D}{T} \tag{11}$$

174 Substituting equation (11) in (10) and integrating we get,

$$lnK = \frac{-J}{RT} + \Delta A lnT + \frac{\Delta B}{2}T + \frac{\Delta C}{6}T^2 + \frac{\Delta D}{2T^2} + I \tag{12}$$

175 From equation (9) and (12) the dependence of ΔG on temperature can be written as:

$$\Delta G^0 = J - RT \left(\Delta A lnT + \frac{\Delta B}{2}T + \frac{\Delta C}{6}T^2 + \frac{\Delta D}{2T^2} + I \right) \tag{13}$$

176 where the data for constants $\Delta A, \Delta B, \Delta C, \Delta D$ can be obtained from [38]. The constants J and I are calculated from

177 equations (11) and (13) at temperature of 298 K.

178   By incorporating the tabulated values and constants the expression for equilibrium constants obtained are:

$$lnK_1 = \frac{5872.39}{T} + 1.86 lnT - 2.7 \times 10^{-4}T - \frac{58200}{T^2} - 18.01 \tag{14}$$

$$lnK_2 = \frac{7083.41}{T} - 6.567lnT + 3.733 \times 10^{-3}T - 3.6 \times 10^{-7} + \frac{35050}{T^2} + 32.5 \qquad (15)$$

179   To obtain the gasification temperature, the energy balance is used:

$$\Delta h_{f,feedstock} + nh^0_{f,H_2O} + wh^0_{f,H_2O} + mh^0_{f,O_2} + 3.76mh^0_{f,N_2} \qquad (16)$$

$$= x_1\left(h^0_{f,H_2} + C_{p,H_2}\Delta T\right) + x_2\left(h^0_{f,CO} + C_{p,CO}\Delta T\right)$$

$$+ x_3\left(h^0_{f,CO_2} + C_{p,CO_2}\Delta T\right) + x_4\left(h^0_{f,H_2O} + C_{p,H_2O}\Delta T\right)$$

$$+ x_5\left(h^0_{f,CH_4} + C_{p,CH_4}\Delta T\right) + \left(\frac{z}{2} + 3.76m\right)\left(h^0_{f,N_2} + C_{p,N_2}\Delta T\right)$$

180   where h_f is the enthalpy of formation and $\Delta T = T - T_{ref}$ where T_{ref} is 298 K.

181   The data for heat of formation of all the species involved in equation (16) can be obtained from JANAF

182   thermochemical tables [39]. The specific heat, C_p, as a function of temperature can be expressed as [38]:

$$C_p = R\left[A + BT_{av} + \frac{C}{3}\left(4T^2_{av} - T_{ref}T\right) + \frac{D}{T_{ref}T}\right] \qquad (17)$$

183   where A, B, C, D are tabular values and $T_{av} = \left(T_{ref} + T\right)/2$.

184   The model was developed in FORTRAN programming language, with the solution of the non-linear

185   equations being achieved using the Newton-Raphson method. The solution procedure for the thermodynamic

186   equilibrium model can be found in Jarungthammachote and Dutta [31].

187

188   **2.1.1.   Verification and validation**

189   For the verification exercise, the results of syngas composition of the present model are compared with the results

190   of the numerical model developed by Jarungthammachote and Dutta [31] for gasification of rubber wood as a

191   biomass feedstock. The comparison is made by setting the gasification temperature fixed at 1100 K for moisture

192   contents of 16% and 14% with air supply rates of 0.4647 and 0.4591 kmole per kmole of biomass, respectively.

193   Fig. 3 shows that the results from both models are in excellent agreement with each other. This consolidates the

194   accuracy of the computational algorithm developed for thermodynamic equilibrium model for gasification.

(a)

(b)
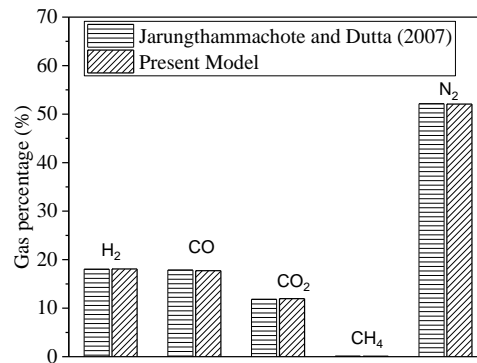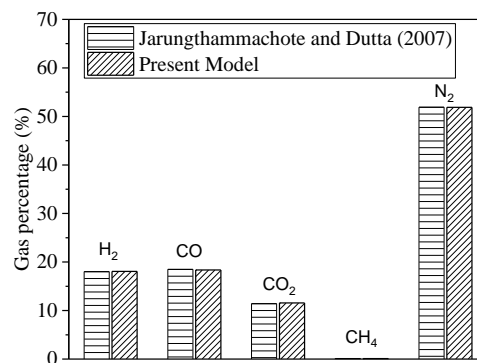
Fig. 3. Comparison of the results obtained using the developed model with the model developed by Jarungthammachote et al. [31] for different air to fuel ratios and moisture contents in rubber wood at a fixed temperature of 1100 K: (a) m = 0.4647, moisture content = 16%; (b) m = 0.4591, moisture content = 14%

The model is further compared with the experimental data on gasification of lignite reported by Patel et al. [36]. The results obtained are for air supply of 0.45 kmole at a fixed gasification temperature of 1100 K. Fig. 4 shows reasonable agreement with the results of the model and the experimental data. The slight deviation in results can be attributed to assumptions such as ideal gas behaviour, modelling of different reaction zones as a single zone, absence of tar etc. The lower concentration of methane is because the methanation reaction does not reach equilibrium at higher temperatures.

205
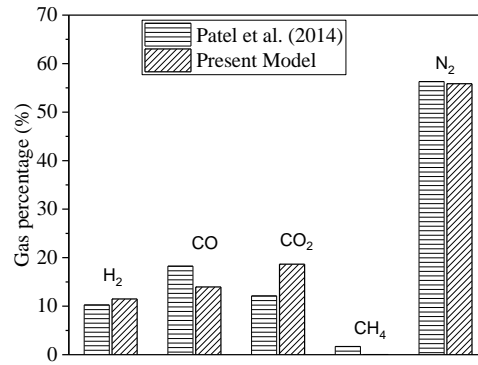
Fig. 4. Comparison of the results using the developed model with the experimental results by Patel et al. [36] for

gasification of lignite

2.2. COMPASS Code

The governing equations of the coupled thermal, hydraulic, chemical and mechanical framework of the

COMPASS code to study the behaviour of unsaturated soils have already been provided elsewhere [28, 29, 33,

40]. Furthermore, the governing equations for the reactive transport of multicomponent gas in a single porosity

unsaturated medium have been given in Sedighi et al. [41], assuming an ideal gas behaviour. Hosking et al. [30]

presented the governing equations for multicomponent reactive chemical transport in dual porosity geomaterials

as well as the aspects related to non-ideal gas flow at high pressures.

For the purpose of this work, a coupled thermal-chemical model of the COMPASS framework has been

used. The existing thermal model was further extended to incorporate temperature dependence of gas conductivity

as well as to consider the variations of thermal conductivity and heat capacity with temperature of different porous

media adopted in this study. Furthermore, geochemical reactions are included via the sorption/desorption module

of the COMPASS code to study the effect of sorption on gas transport.

The governing equation of heat transfer has been developed based on the energy conservation law in

$$\frac{\partial}{\partial t}[H_c(T - T_R)] = -\nabla \lambda_T \nabla T \qquad (18)$$

where H_c is the heat storage capacity, T is the soil/rock temperature, T_R is a reference temperature, and λ_T is the

thermal conductivity. Heat convection is neglected in this work due to the dominate role of heat conduction in

low permeability medium [42].

225   A mass conservation equation is applied to derive the multicomponent gas chemical transport in which the

226   temporal derivative of the gas chemical accumulation is equal to the spatial gradient of the flux. A sink/source

227   term is added allowing for chemical reactions. The governing equation is given by:

$$\frac{\partial}{\partial t}[\theta c_g^i] + R^i = -\nabla[c_g^i v_g] + \nabla[D^i \nabla c_g^i] \tag{19}$$

228   where c_g^i is the ith gaseous chemical component and D^i is the effective diffusion coefficient derived from the free

229   fluid diffusion coefficient to account for the tortuous diffusion paths in a porous medium [30]. θ is the volumetric

230   gas content represented by multiplying porosity n and degree of gas saturation S_g.

231   Using Darcy's law for the advective flux, the expression for v_g is:

$$v_g = -k\left[\nabla \frac{u_g}{\rho_g g} + \nabla z\right] \tag{20}$$

232   where z is the elevation and k is the gas conductivity which can be expanded to give:

$$k = \frac{K \rho_g g}{\mu_g} \tag{21}$$

233   where K is the intrinsic permeability and μ_g is the absolute gas viscosity which is included using the approach in

234   which viscosity depends on composition, temperature and pressure [30]. The viscosity model is expressed as:

$$\mu_g = 0.1[f(\mu_g^0) + \mu_g^D] \tag{22}$$

235   where $f(\mu_g^0)$ is a function of the gas mixture viscosity at low pressure and μ_g^D is an adjustment for dense gases.

236   The bulk gas pressure, u_g, can be expressed in terms of the sum of concentrations of the chemical

237   components in the gas phase, given by:

$$u_g = ZRT \sum_{j=1}^{n_g} c_g^j \tag{23}$$

238   where Z is the compressibility factor (equal to 1 in ideal gas case), R is the universal gas constant, T is the

239   temperature, and n_g is the number of gas components.

240   Development of a sink/source term for chemical reactions, R^i, is limited here to adsorption and desorption

241   of gases by solids and can be expressed as:

$$R^i = \rho_s \frac{\partial s^i}{\partial t} \tag{24}$$

242   where ρ_s is the dry bulk density of the solid and s^i is the adsorbed amount of the ith chemical component which

243   has been calculated using the extended Langmuir isotherm [30]:

$$s^i = \frac{n^i b_L^i ZRT c_g^i}{1 + ZRT \sum_{j=1}^{n_g} b_L^j c_g^j} \tag{25}$$

244   where n^i is the Langmuir capacity and b_L^i is the reciprocal of the Langmuir pressure. In this approach, it is

245   assumed that the sorption process is sufficiently fast compared to the transport speed. Hence, the local chemical

246   equilibrium between the adsorbed gas phase and the free gas phase is considered to exist.

247   A numerical solution of the two governing partial differential equations is achieved with the finite element

248   method for spatial discretisation and the finite difference method for temporal discretisation [28, 29, 33, 40]. The

249   THCM model of the COMPASS code has been extensively verified, validated and applied for a range of geo-

250   environmental/geo-energy applications. In regards to the thermo-chemical model used in this work, the thermal

251   aspects of the model have been verified against analytical solutions and validated against experimental data on

252   heat propagation in various types of soils and rocks [34, 43, 44]. Also, the multicomponent high pressure ideal

253   and real gas transport and its sorption in coal have been verified against analytical solutions for pure diffusive and

254   advective-diffusive gas transport as well as the comparison of simulation results with those presented in the

255   literature for an alternative numerical model and validated against experimental data [30, 45]. Details of the

256   numerical formulation and computational aspects have been discussed in previous publications mentioned above

257   and therefore, the details are not repeated here.

258

259   **3.   Problem setup**

260   During underground coal gasification, the process gas will tend to escape from the cavity if there is an outward

261   pressure gradient. In order to prevent this, a common practice is to ensure that the fluid flow from the strata

262   surrounding the cavity must be towards it [46]. However, under specific conditions where coal acts as a confined

263   aquifer surrounded by low permeability strata, a layer of unreacted coal may exist around the upper part of the

264   cavity where the surrounding coal drains off water and the pores are partially filled with gas [46]. This is

265   schematically shown in Fig. 5. The zone of unreacted coal could be extended even further in dipping coal seams

266   where the gas could flow a long distance in the up-dip direction [46].
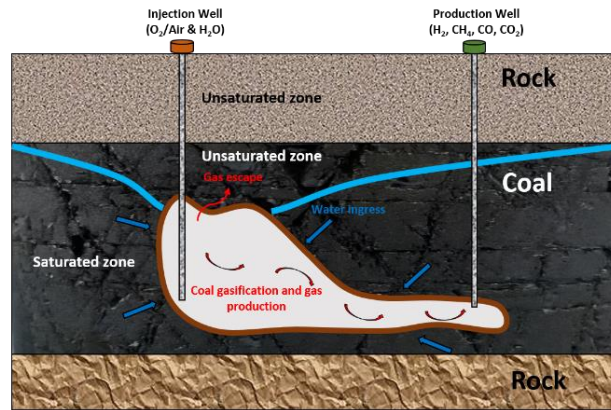
Fig. 5. Potential of gas escape where a shoulder of unreacted coal may exist in the upper part of the coal seam surrounding the cavity (adapted from Camp and White [46])

This work is therefore trying to provide further understanding of how the amount of water injected into the cavity affects the concentration of the individual syngas components and the reaction temperature. Furthermore, it is studied how the primary product gases, i.e. methane, hydrogen, carbon monoxide, carbon dioxide and nitrogen, flow through the overlying strata. As methane and carbon dioxide are very potent greenhouse gases, it is also investigated whether sorption of these gases on the surrounding rock, upon their potential escape from the cavity, can retard their propagation and provide a potential for their storage.

3.1. Domain and material properties

Coal seams are often overlaid by low permeable rocks such as shales and mudstones, and more permeable sandstones which is also the case for the South Wales Coalfied [47]. A recent study of the South Wales coalfield through exploratory drilling for environmental monitoring purposes has suggested that samples from various depths exhibit mineralogic characteristics of shale deposits and that several thick coal seams are overlaid by sandstone layers [48]. Furthermore, through continuous monitoring of ground water level in the boreholes in a duration of more than 2.5 years, it was shown that the water level in one of the boreholes is around 350 m below the surface [48]. Therefore, a sensitivity analysis considering gas flow through mudstone/shale, sandstone and coal in partially dry conditions, assuming the degree of water saturation of 0.61 as a reasonable value for the materials studied [49-51], has been considered in this study to reflect the real geological conditions experienced in the coalfield.

The system is represented as a 30 m long domain with 1 m height, discretised into 300 equally-sized 4-noded quadrilateral elements. A summary of the material parameters is given in Table 1. As shown in the table,

291 thermal conductivity and heat capacity of the materials studied have been considered as a function of temperature.

292 Several studies conducted analyses of gas sorption in porous geo-materials over a range of temperatures, on coals

293 up to 350 K [52] and shales up to 318 K [53], and have suggested that the sorption capacity decreases with an

294 increase in temperature as the sorption is an exothermic process [52, 53]. However, literature data on the sorption

295 of different gases under high-temperature conditions that can be experienced in the surroundings of the UCG

296 cavity is very scarce. Hence, in this work the sorption properties of different materials represent sorption at

297 isothermal conditions. Sorption data at the temperature of 313 K and 318 K are adopted for the cases of CO_2 and

298 CH_4 on coal, respectively. Sorption of the same gases on shale is taken at 318 K, while the sorption of CO_2 and

299 CH_4 on sandstone is represented at 323 K and 296 K, respectively. It should be noted that the sorption parameters

300 for shale and sandstone were obtained by fitting the Langmuir curve to the experimental data provided in the

301 literature (Table 1).

302

303 **3.2. Model parametrization and boundary conditions**

304 The thermodynamic equilibrium model is used to analyse the effect of steam supply ranging from 0.35 to 1.55

305 kmol on the product gas composition and the reaction temperature. Furthermore, air is considered to be a primary

306 gasifying agent at a constant injection of 0.5 kmol. Coal properties of an anthracite coal from the South Wales

307 coalfield have been used as an input for the thermodynamic equilibrium model. For that purpose, Proximate and

308 ultimate analysis data given in Table 2 have been used [54].

309 Based on the results provided by the thermodynamic equilibrium model, a scenario generating the highest

310 amount of CO_2 and CH_4 is used as input, i.e. boundary condition for the reactive transport model of the COMPASS

311 code. Initial and downstream boundary conditions are assumed to be atmospheric. The simulation considered an

312 arbitrary injection pressure of 20 bar which would represent UCG at a minimum depth of 200 m below ground

313 level. The simulation period is 30 days.

314 **4. Results and discussion**

315 In this section, the simulation results on gasification temperature and syngas formation as well as heat and gas

316 propagation through different porous media obtained using the thermo-chemical model of the COMPASS code

317 are presented. Subsequently, the results on gas propagation in the same porous media are shown and analysed

318 with emphasis on the effect of gas sorption on gas transport.

319

320

321 Table 1. Parameter values used in simulations

Material parameters	Sandstone	Coal	Shale/Mudstone
Porosity [%]	25 [55]	25 [56]	25 [57]
Permeability [mD]	1.0 [58]	0.1 [34]	0.01 [57]
Density [kg.m^{-3}]	2650 [58]	1376 [34]	2316 [59]
Thermal conductivity [W.m^{-1}.K^{-1}]	$\lambda = {}^{1}/_{(0.000497 * T + 0.764518)}$ [60]	$\lambda = 3 * 10^{-6} * T^2 - 0.001 * T + 0.2625$ [61]	$\lambda = {}^{1}/_{(0.000288 * T + 0.749849)}$ [60]
Heat capacity [J.kg^{-1}.K^{-1}]	810 [60]	$C_p = -0.001 * T^2 + 2.1418 * T + 854.83$ [61]	$C_p = 0.0007 * T^2 - 1.1434 * T + 1336$ [60]
Langmuir pressure (CO_2) [MPa]	2.83 [62]	0.61 [54]	1.0 [53]
Langmuir capacity (CO_2) [mol/kg]	0.49 [62]	1.73 [54]	0.285 [53]
Langmuir pressure (CH_4) [MPa]	3.86 [63]	1.2 [52]	1.71 [53]
Langmuir capacity (CH_4) [mol/kg]	0.175 [63]	1.52 [52]	0.184 [53]

322

323 Table 2. Proximate and ultimate characteristics of coal considered in the model simulations [54]

Proximate analysis		Ultimate analysis	
Moisture content	0.91%	Total carbon content	89.5%
Ash	4.62%	Sulphur content	0.87%
Volatile matter	5.73%	Hydrogen content	3.16%
Fixed carbon content	88.7%	Nitrogen content	1.31%
		Oxygen content	0.33%

324

4.1. Reactive transport boundary conditions

326 The results of the thermodynamic model are given in Fig. 6 and 7. It is shown in Fig. 6 that steam supply affects

327 the gasification temperature, i.e. increase in the amount of steam submitted to the system decreases the temperature

328 in the UCG cavity by 115 K, i.e. from 1224 K to 1109 K for the range of the steam supply considered. This is

329 related to the fact that steam gasification is a highly endothermic reaction which favours the generation of

330 hydrogen. This can be confirmed from Fig. 7 where it is visible that an increase in steam supply benefits the

331 hydrogen and methane production, while it reduces the concentration of carbon monoxide generated. In particular,

332 the concentration of hydrogen increases from 11.9% to 17.75%, concentration of methane from 0.35% to 1.62%

333 and concentration of carbon monoxide decreases from 23.59% to 10.17%. However, the CO_2 concentration
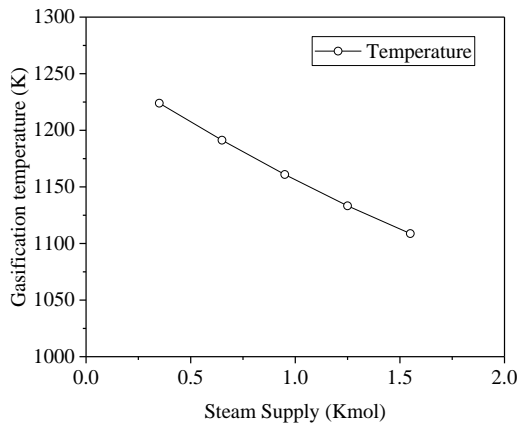
334

335   Fig. 6. The effect of steam supply on the gasification temperature
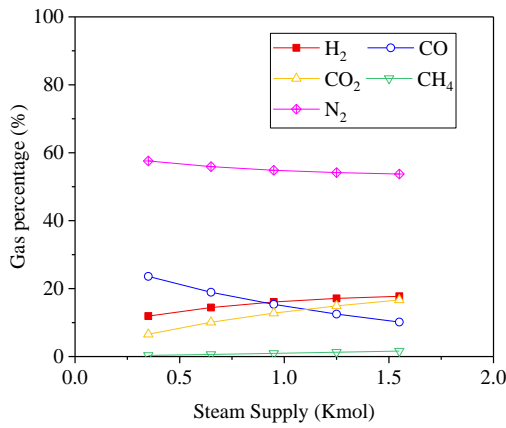
336

337   Fig. 7. The effect of steam supply on the syngas composition (on dry basis)

338

339   Table 3. Reactive transport boundary conditions

Upstream boundary conditions	Initial conditions	Downstream boundary conditions
Fixed gas concentrations at 20 bar:	Initial gas concentrations at 1bar:	Fixed gas concentrations at 1 bar:
C_g (CO_2) = 36.19 mol.m^{-3}	C_g (CO_2) = 0 mol.m^{-3}	C_g (CO_2) = 0 mol.m^{-3}
C_g (CH_4) = 3.51 mol.m^{-3}	C_g (CH_4) = 0 mol.m^{-3}	C_g (CH_4) = 0 mol.m^{-3}
C_g (H_2) = 38.51 mol.m^{-3}	C_g (H_2) = 0 mol.m^{-3}	C_g (H_2) = 0 mol.m^{-3}
C_g (CO) = 22.06 mol.m^{-3}	C_g (CO) = 0 mol.m^{-3}	C_g (CO) = 0 mol.m^{-3}
C_g (N_2) = 116.59 mol.m^{-3}	C_g (N_2) = 32.31 mol.m^{-3}	C_g (N_2) = 32.31 mol.m^{-3}
	C_g (O_2) = 8.59 mol.m^{-3}	C_g (O_2) = 8.59 mol.m^{-3}
Fixed temperature:	Initial temperature:	Fixed temperature:
T = 1108.75 K	T = 298 K	T = 298 K

340 increases from 6.57% to 16.68%. Hence, small amounts of steam injection should be encouraged since net

341 calorific value of syngas increases based on increase in yield of H_2 and CH_4. Higher methane yield is obtained if

342 gasification takes place at lower temperatures and higher pressure. Higher amounts, then considered in this study,

343 of steam injection should be avoided owing to drop in CO and increase in CO_2 concentration. As mentioned, the

344 simulation results providing the highest amounts of CO_2 (16.68%) and CH_4 (1.62%) as well as the corresponding

345 gasification temperature of 1108.75 K are used as boundary conditions for the reactive transport model to analyse

346 the heat and gas propagation in different porous media surrounding the UCG cavity. A complete overview of the

347 reactive transport boundary conditions is given in Table 3.

348   **4.2. Heat transport**

349 Fig. 8 shows the temperature distribution in the domain at the end of the studied period. It can be observed that

350 for the different geological formations considered in this study, the influenced areas of temperature are limited to

351 round 5.0 m. As the heat transfer in this work was governed by conduction only, some minor differences can be

352 observed due to the different thermal conductivities and heat capacities of three materials considered in this study,

353 as indicated in Table 1.
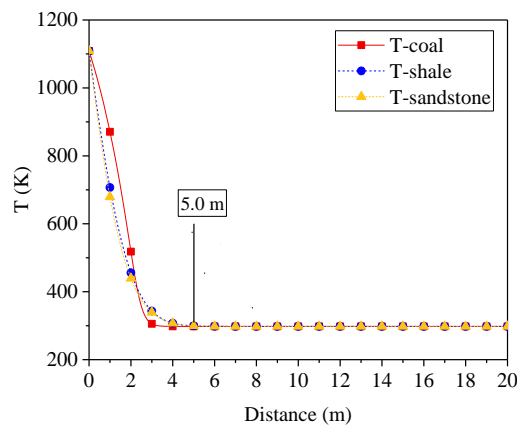
354

355 Fig. 8. The distribution of temperature after 30 days in different porous media

356

357   **4.3. Gas propagation**

358 The propagation of syngas components in different porous media at the end of the studied period is given in Fig.

359 9, where the transport of CO_2, CH_4, H_2, CO and N_2 is presented in Fig. 9a, 9b, 9c, 9d and 9e, respectively.

360   Fig. 9a shows that CO_2 reaches the distance of 16.0 m in sandstone, which is further in comparison to gas

361 propagation up to 6.8 m in coal and 5.9 m in shale. For other gases studied in Fig.9b, 9c, 9d and 9e, it can also be

362 observed that the gas front in the sandstone is located further than in coal and shale. In addition, the gas front of

363   CO_2, CH_4, CO and N_2 is minimum 8.6 m and 5.9 m for H_2 further in sandstone compared to other materials (coal

364   and shale). Such observation is mainly related to the difference in intrinsic permeabilities of different porous

365   media (sandstone 1mD > coal 0.1 mD > shale 0.01mD), leading to the differences of gas conductivities which

366   controls the gas advection in porous media.

(a)

(b)

(c)

(d)

(e)
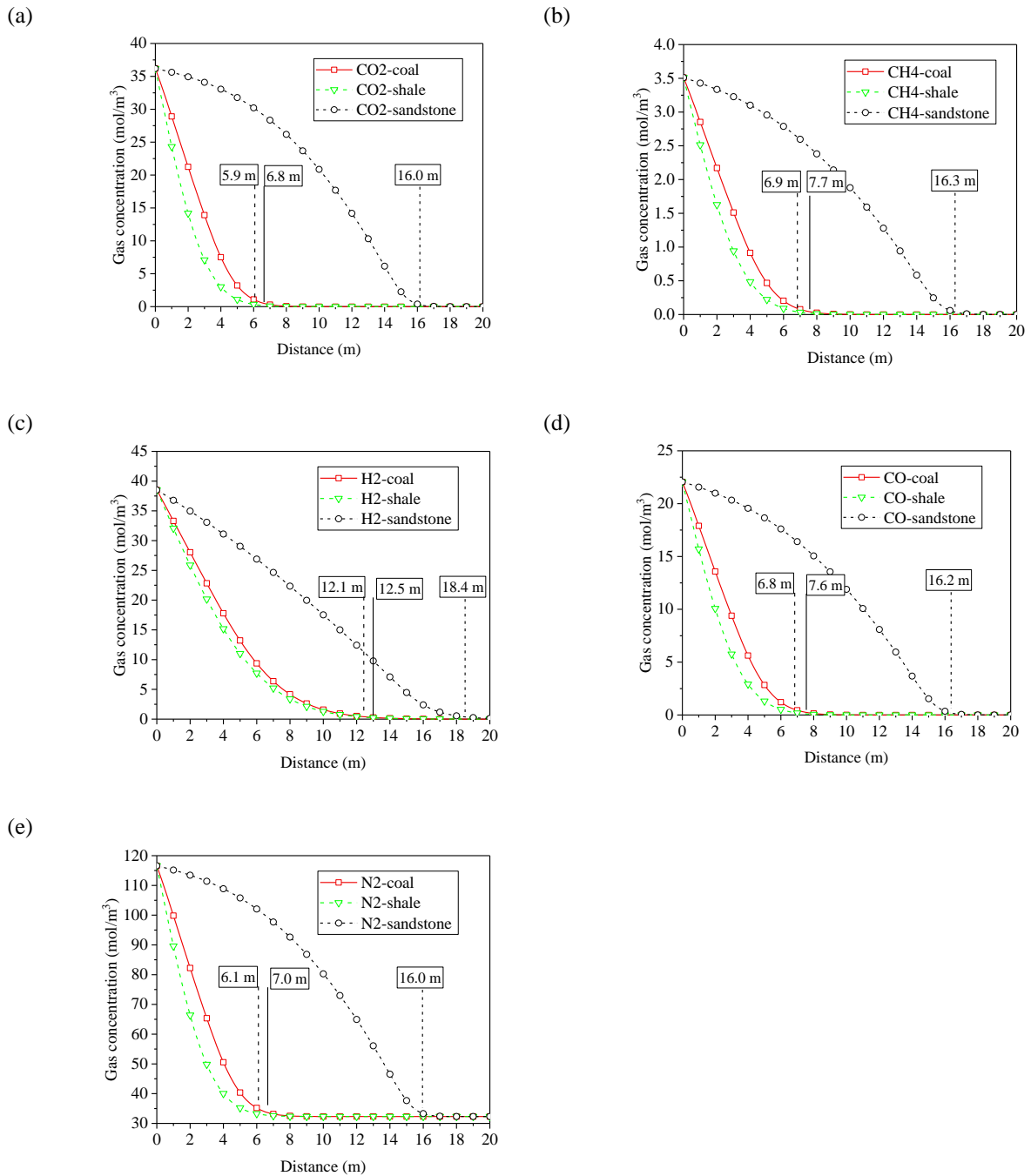
367   Fig. 9. Concentration of five different syngas components at the end of studied period (30 days) in three different

368   porous media: coal, shale and sandstone: (a) Carbon dioxide, (b) Methane, (c) Hydrogen, (d) Carbon monoxide

369   and (e) Nitrogen

370

371   In sandstone, gas front of H_2 is located at 18.4 m, further than that of CO_2, CH_4, CO and N_2, which are 16.0 m,

372   16.3 m, 16.2 m, and 16.0 m, respectively. Similar gas propagation can also be observed in coal and shale. The

373   reason why H_2 propagates further in the domain than other gases is related closely to the gas diffusion coefficients.

374   CO_2, CH_4, CO and N_2 have very similar diffusion coefficients: 1.42×10^{-5} m^2/s for CO_2, 1.96×10^{-5} m^2/s for CH_4,

375   1.9×10^{-5} m^2/s for CO, and 1.5×10^{-5} m^2/s for N_2, while the diffusion coefficient of H_2 (6.11×10^{-5} m^2/s) is

376   approximately 5 times higher compared to other gases. It was stated by Nazaroff and Sextro [64] that the

377   importance of gas diffusion increases when the permeability value of porous media is lower than 1.7×10^{-11} m^2.

378   Hence, both gas diffusion and advection contribute to the gas transport in these three porous media, but gas

379   diffusion plays a higher role than gas advection in the cases of coal and shale. Despite one order of magnitude

380   difference in intrinsic permeability values of coal and shale, the location of gas breakthrough fronts differ between

381   0.4 to 0.9 m, depending on the gas considered. However, it appears that advection and diffusion are competing

382   mechanisms in sandstone as, despite the same porosity of shale and sandstone, gas fronts differ up to 9.2 m.

383   **4.4. Effect of sorption on gas flow**

384   It is observed in Fig. 10a that the gas front of CO_2 in coal is located at round 6.8 m from the injected surface.

385   When gas adsorption is considered, the Langmuir pressure, which is the pressure at which one half of the

386   Langmuir volume can be adsorbed [65], plays an important role in the gas distribution. The total gas pressure in

387   the case without adsorption is presented in Fig. 10c. At the injection face, gas pressure is 2.0 MPa, much higher

388   than the Langmuir pressure of CO_2 in coal (0.61 MPa), leading to quick adsorption of CO_2 at a distance of 0.2 m

389   and a very low CO_2 concentration at greater distance from the injection site. In terms of CH_4 (Fig. 10b), its gas

390   front is located at the distance of 7.7 m for the case of non-adsorption and 0.5 m under consideration of adsorption

391   due to the higher total gas pressure at the injection face compared to the Langmuir pressure of CH_4 in coal (1.2

392   MPa). Therefore, the similar variation tendency of CO_2 can also be identified for CH_4, presenting the importance

393   of adsorption in the study of gas transport.

(a)

(b)

(c)
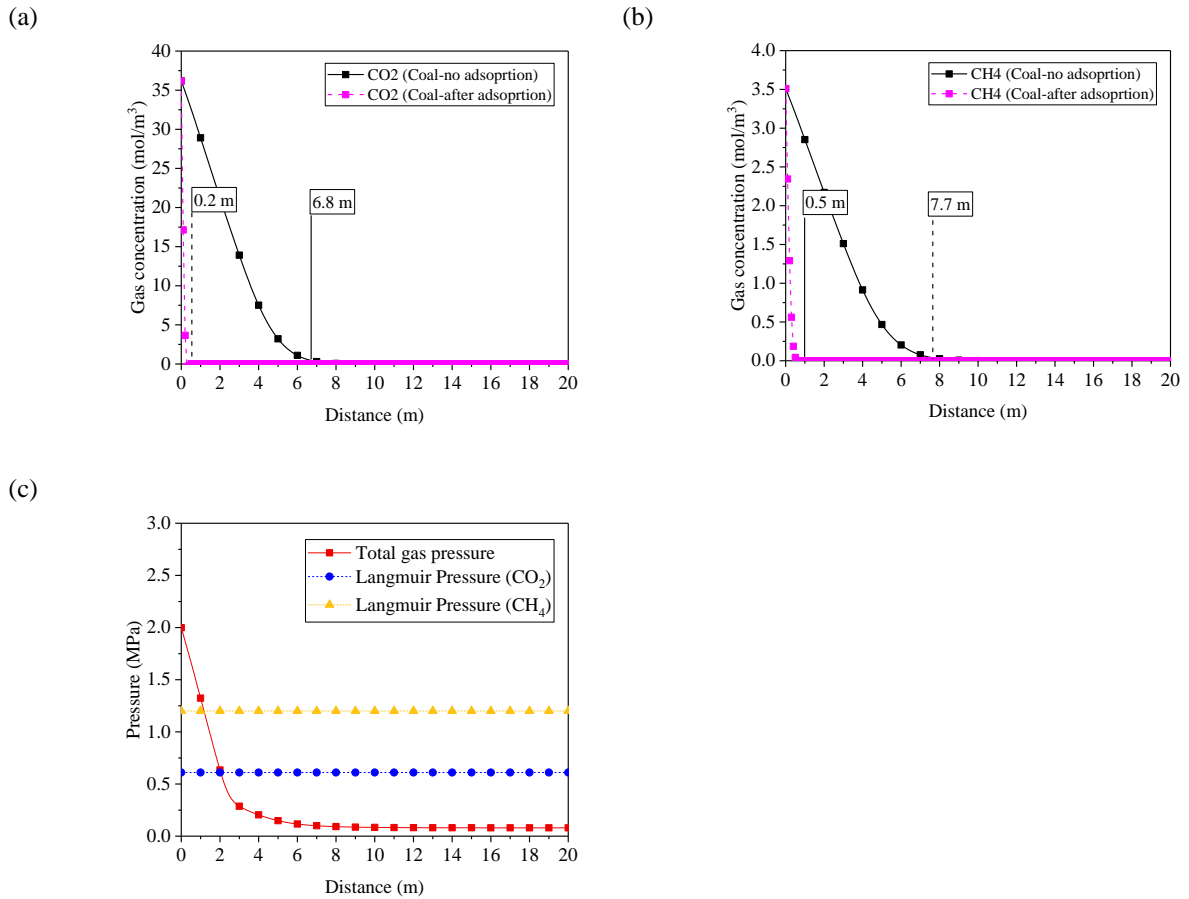
Fig. 10. The distribution of gas concentrations in coal with and without considering gas sorption at day 30: (a) Carbon dioxide, (b) Methane and (c) total gas pressure in the case without adsorption

The distribution of CO_2 concentrations in shale with and without adsorption is presented in Fig. 11a. The gas front positions in the cases of no adsorption and with considering adsorption are 5.9 m and 0.8 m, respectively. Fig. 11b shows the gas propagation of CH_4 in shale with and without adsorption, allowing a gas front move to 1.8 m and 6.9 m, respectively. It can be observed in Fig. 11c that the total gas pressure (2.0 MPa) is larger than the Langmuir pressure of CO_2 (1.0 MPa) and CH_4 (1.71 MPa) in shale, leading to the efficient adsorption of gases in the first 0.8 m and 1.8 m distances, respectively.

(a)

(b)

(c)
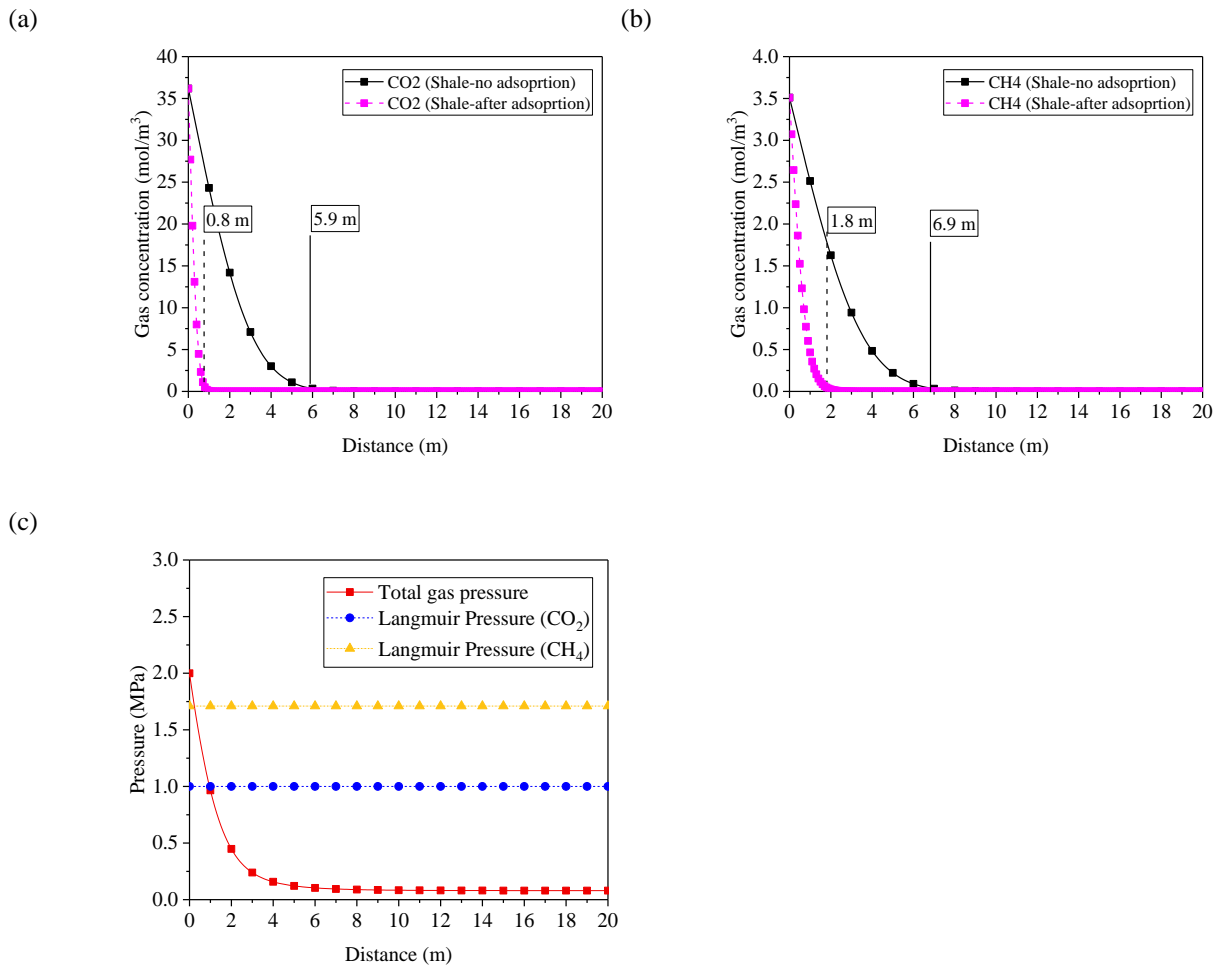
403   Fig. 11. The distribution of gas concentrations in shale with and without considering the gas sorption at day 30:

404   (a) Carbon dioxide, (b) Methane and (c) total gas pressure in the case without adsorption

405

406   Fig. 12a illustrates the distribution of CO_2 in sandstone with and without consideration of adsorption,

407   presenting the gas fronts located at 1.4 m and 16.0 m, respectively. Langmuir pressure of CO_2 (2.83 MPa) is

408   slightly larger than the total gas pressure at the injection face (Fig. 12c). Thus, CO_2 is absorbed efficiently and its

409   concentration decreases to smaller values at the distance of 1.4 m. However, the Langmuir pressure of CH_4 (3.86

410   MPa) is larger than the total gas pressure at the injection face, leading to further transport of CH_4, up to 4.1 m, in

411   sandstone compared to that of CO_2 (Fig. 12b).

(a)

(b)

(c)
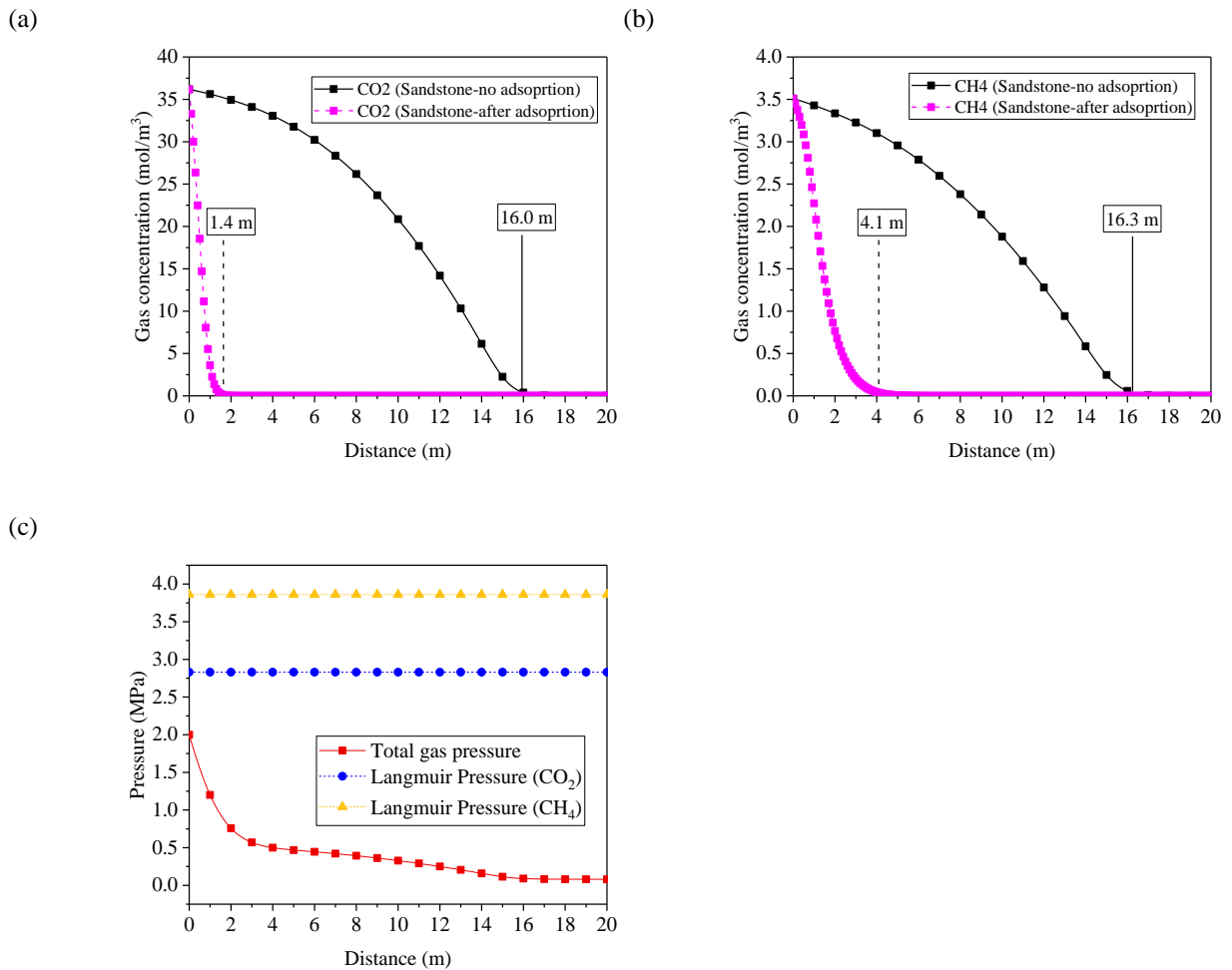
412   Fig. 12. The distribution of gas concentrations in sandstone with and without considering the gas sorption at day

413   30: (a) Carbon dioxide, (b) Methane and (c) total gas pressure in the case without adsorption

414

415   As shown above, Langmuir pressure values considered in this study have a strong impact on the amount

416   of adsorbed gases. However, the equilibrium modelling approach taken in this work to consider sorption also has

417   an impact on the sorbed amount. Using the equilibrium sorption approach, it is assumed that the sorbed amount

418   in the rock matrix is in equilibrium with the free gas concentrations in the pores and fractures [54]. This means

419   that applying a fixed concentration boundary would cause instantaneous sorption at the boundary and reduction

420   of the free gas concentration. However, as gas adsorption is known to be a kinetic reaction, which would include

421   gas exchange between the fractures and the rock matrix, diffusion through the matrix and sorption of the gas

422   molecules on the sorption sites, the equilibrium behaviour is only partially realistic. Implementing a kinetic

423   approach would require further research investigations to obtain a good understanding of the relationship between

424   the adsorbed amount at non-equilibrium conditions for the range of porous media considered in this study.

425   Therefore, the equilibrium approach is adopted for the preliminary study in this paper and provides novel insights

426   into the effect of gas sorption on gas transport.

427   Another important aspect related to gas sorption is the potential of the host rock to swell under the

428   conditions of gas sorption, which is particularly pronounced in coals compared to shale and sandstone. Swelling

429   of the porous media is understood to be strongly correlated with the sorption amount [66]. The sorption-induced

430   swelling often results in closure of the existing flow paths, thus reducing the permeability of the porous medium

431   and affecting the gas propagation [54]. It would have positive implications for retarding the potential gas escape

432   in the surrounding strata of UCG, especially if there are coal seams located at a certain distance above the UCG

433   reactor which would then act as a barrier. Thereby, considering sorption and rock swelling for UCG surrounding

434   strata would provide a potential not just to retard the gas propagation, but also to provide geological storage of

435   the leaked specific syngas components, such as CH_4 and CO_2.

436   As mentioned previously, gas sorption is a temperature dependent process, i.e. the sorption capacity

437   decreases with an increase in temperature [52]. Hence, future experimental and theoretical studies should be

438   undertaken to provide further understanding on the impact of high temperatures experienced during the UCG

439   process on the sorption potential of the UCG products. In conclusion, the cases with and without consideration of

440   adsorption of CO_2 and CH_4 in three different porous media (coal, shale and sandstone) are well analysed depending

441   on their Langmuir isotherms, reflecting the effect of adsorption on the gas propogation and the significance to

442   consider adsorption in the study of gas transport.

443

444   **5.   Conclusions**

445   In this study, the thermodynamic equilibrium model is developed and applied to analyse the effect of gasification

446   reagents on the syngas composition and gasification temperature as well as to provide thermal and chemical (gas)

447   boundary conditions for the coupled thermo-chemical model contained within the thermo-hydraulic-chemical-

448   mechanical framework of the COMPASS code. The code is then used to study the variations of temperature and

449   gas concentrations, considering the reactive gas transport mechanisms, in three different porous media (coal, shale

450   and sandstone) surounding the UCG reactor.

451   Based on the the simulation results on coal gasification conducted under constant pressure conditions (20

452   bar) and constant air supply (0.5 kmol), it can be concluded that to achieve a syngas with high contents of methane

453   and hydrogen, an excess of steam above the stoichiometric on a molar basis for primary gasification reactant (e.g.

454   air in this study) is recommended. However, this comes at a potential cost of reducing the overall calorific value

455 of the syngas as the concentration of CO, a gas with high calorific value, significantly decreases. Furthermore,

456 higher amounts of steam in the system increase the concentration of CO_2 in the gas mixture, which poses an

457 environmental concern and increases the costs associated with CO_2 utilisation and storage once it is collected at

458 the surface facility.

459 By studying the transport of a gas mixture under the scenario of a potential gas migration from the UCG

460 reactor into the surrounding strata, it can be inferred that both gas diffusion and advection have a significant role

461 in the gas transport in such low permeable porous media considered in this study. In particular, gas diffusion and

462 advection are competing transport mechanisms in porous media with intrinsic permeability higher than 1 mD

463 (sandstone), while the gas diffusion becomes a dominant transport process in porous media with an intrinsic

464 permeability lower than 1 mD (coal and shale). Such results confirm the importance of considering low

465 permeability strata surrounding the UCG reactor, widely recognised in the literature [16, 46], which can act as an

466 effective barrier to contain the contaminants generated and potentially leaked during the UCG process.

467 Moreover, the study of gas adsorption of highly potent greenhouse gases, i.e. methane and carbon dioxide

468 by porous media, emphasised the significance of considering the adsorption effect in the gas transport in the

469 overall UCG process. Based on the simulation results presented, it can be concluded that the sorption of gases can

470 retard their propagation in the strata surrounding the UCG cavity which is particularly significant in materials

471 with high affinity to gases, such as coals and shales. Such observations then suggest that the coal pillars separating

472 UCG reactors in a multi-well UCG configuration or shale layers located above the UCG target seams, commonly

473 intersected by thinner coal seams, would adsorb some of the gas that could potentially leak. Although the gas

474 sorption is a temperature-dependent kinetic process which is not fully considered in this work due to the lack of

475 available data, this work provides further insights on the importance of considering the adsorption to understand

476 the gas migration in the area around the UCG reactor.

477 With the background of rapid-developed UCG technology and the development of integrated UCG models

478 focusing on syngas production, coal conversion rates and cavity shape, it has been widely suggested that future

479 work should focus on the development of numerical tools capable to simulate and optimise the production and

480 composition of the syngas and the environmental and geo-mechanical impacts of UCG products in complex well

481 configurations [2, 3]. Hence, this study contributes to such work by presenting a numerical framework capable of

482 studying the formation of UCG products and its reactive transport in the geological formations surrounding the

483 UCG reactor to address the environmental issues of complicated UCG process, aid in managing the environmental

484   practices, reducing pollution risk and securing greater public and regulatory support for the UCG
485   commercialization.

486

491

492   **7. References**

493   1.   Bhutto, A.W., A.A. Bazmi, and G. Zahedi, *Underground coal gasification: From*
494   *fundamentals to applications.* Progress in Energy and Combustion Science, 2013.
495   **39**(1): p. 189-214.

496   2.   Khan, M.M., et al., *Modelling underground coal gasification—A review.* Energies, 2015.
497   **8**(11): p. 12603-12668.

498   3.   Perkins, G., *Underground coal gasification–Part II: Fundamental phenomena and*
499   *modeling.* Progress in Energy and Combustion Science, 2018. **67**: p. 234-274.

500   4.   Andrianopoulos, E., A. Korre, and S. Durucan, *Chemical process modelling of*
501   *underground coal gasification and evaluation of produced gas quality for end use.*
502   Energy Procedia, 2015. **76**: p. 444-453.

503   5.   Andrianopoulos, E., et al., *Coupled Thermo-Mechanical-Chemical modelling of*
504   *underground coal gasification*, in *Computer Aided Chemical Engineering.* 2016,
505   Elsevier. p. 1069-1074.

506   6.   Perkins, G. and V. Sahajwalla, *Steady-state model for estimating gas production from*
507   *underground coal gasification.* Energy & Fuels, 2008. **22**(6): p. 3902-3914.

508   7.   Perkins, G. and V. Sahajwalla, *Modelling of heat and mass transport phenomena and*
509   *chemical reaction in underground coal gasification.* Chemical Engineering Research
510   and Design, 2007. **85**(3): p. 329-343.

511   8.   Seifi, M., J. Abedi, and Z. Chen, *Application of porous medium approach to simulate*
512   *UCG process.* Fuel, 2014. **116**: p. 191-200.

513   9.   Duan, T.-H., et al., *Pyrolysis and gasification modelling of underground coal*
514   *gasification and the optimisation of CO2 as a gasification agent.* Fuel, 2016. **183**: p.
515   557-567.

516   10.   Samdani, G., et al., *A process model for underground coal gasification–Part-I: Cavity*
517   *growth.* Fuel, 2016. **181**: p. 690-703.

518   11.   Jiang, L., Z. Chen, and S.F. Ali, *Modelling of reverse combustion linking in*
519   *underground coal gasification.* Fuel, 2017. **207**: p. 302-311.

520   12.   Klebingat, S., et al., *Innovative thermodynamic underground coal gasification model*
521   *for coupled synthesis gas quality and tar production analyses.* Fuel, 2016. **183**: p. 680-
522   686.

523   13.   Klebingat, S., et al., *Optimization of synthesis gas heating values and tar by-product*
524   *yield in underground coal gasification.* Fuel, 2018. **229**: p. 248-261.

525 14. Najafi, M., S.M.E. Jalali, and R. KhaloKakaie, *Thermal–mechanical–numerical*
526   *analysis of stress distribution in the vicinity of underground coal gasification (UCG)*
527   *panels.* International Journal of Coal Geology, 2014. **134**: p. 1-16.

528 15. Elahi, S., M. Nassir, and Z. Chen, *Effect of various coal constitutive models on coupled*
529   *thermo-mechanical modeling of underground coal gasification.* Journal of Petroleum
530   Science and Engineering, 2017. **154**: p. 469-478.

531 16. Sury, M., et al., *Review of environmental issues of underground coal gasification.* WS
532   Atkins Consultants Ltd., University of Liège Belgium, FWS Consultants Ltd, 2004. **126**:
533   p. 1-126.

534 17. Green, M., *Recent developments and current position of underground coal*
535   *gasification.* Proceedings of the Institution of Mechanical Engineers, Part A: Journal of
536   Power and Energy, 2018. **232**(1): p. 39-46.

537 18. Yang, L. and X. Zhang, *Modeling of contaminant transport in underground coal*
538   *gasification.* Energy & Fuels, 2008. **23**(1): p. 193-201.

539 19. Janoszek, T., et al., *Modelling of gas flow in the underground coal gasification process*
540   *and its interactions with the rock environment.* Journal of Sustainable Mining, 2013.
541   **12**(2): p. 8-20.

542 20. Soukup, K., et al., *Modeling of contaminant migration through porous media after*
543   *underground coal gasification in shallow coal seam.* Fuel Processing Technology,
544   2015. **140**: p. 188-197.

545 21. Jiang, L., Z. Chen, and S.F. Ali, *General hydro-geological impact of cleats on*
546   *underground coal gasification.* Fuel, 2018. **224**: p. 128-137.

547 22. Imran, M., et al., *Environmental concerns of underground coal gasification.* Renewable
548   and Sustainable Energy Reviews, 2014. **31**: p. 600-610.

549 23. LIU, S.-q., et al., *Groundwater pollution from underground coal gasification.* Journal of
550   china University of Mining and Technology, 2007. **17**(4): p. 467-472.

551 24. Kapusta, K. and K. Stańczyk, *Pollution of water during underground coal gasification*
552   *of hard coal and lignite.* Fuel, 2011. **90**(5): p. 1927-1934.

553 25. Laciak, M., et al., *The analysis of the underground coal gasification in experimental*
554   *equipment.* Energy, 2016. **114**: p. 332-343.

555 26. Kostúr, K., M. Laciak, and M. Durdan, *Some influences of Underground Coal*
556   *Gasification on the environment.* Sustainability, 2018. **10**(5): p. 1512.

557 27. Upadhye, R., E. Burton, and J. Friedmann, *Science and technology gaps in*
558   *underground coal gasification.* Lawrence Livermore Laboratory, University of
559   California, Livermore, California, 2006. **222523**.

560 28. Thomas, H.R. and Y. He, *Modelling the behaviour of unsaturated soil using an*
561   *elastoplastic constitutive model.* Géotechnique, 1998. **48**(5): p. 589-603.

562 29. Thomas, H.R., M. Sedighi, and P.J. Vardon, *Diffusive reactive transport of*
563   *multicomponent chemicals under coupled thermal, hydraulic, chemical and*
564   *mechanical conditions.* Geotechnical and Geological Engineering, 2012. **30**(4): p. 841-
565   857.

566 30. Hosking, L.J., H.R. Thomas, and M. Sedighi, *A dual porosity model of high-pressure*
567   *gas flow for geoenergy applications.* Canadian Geotechnical Journal, 2017. **55**(6): p.
568   839-851.

569 31. Jarungthammachote, S. and A. Dutta, *Thermodynamic equilibrium model and second*
570   *law analysis of a downdraft waste gasifier.* Energy, 2007. **32**(9): p. 1660-1669.

571 32. La Villetta, M., M. Costa, and N. Massarotti, *Modelling approaches to biomass*
572   *gasification: A review with emphasis on the stoichiometric method.* Renewable and
573   Sustainable Energy Reviews, 2017. **74**: p. 71-88.

574 33. Thomas, H. and P. Cleall, *Inclusion of expansive clay behaviour in coupled thermo*
575   *hydraulic mechanical models.* Engineering Geology, 1999. **54**(1-2): p. 93-108.

576 34. Zagorščak, R., M. Sedighi, and H.R. Thomas, *Effects of Thermo-Osmosis on Hydraulic*
577   *Behavior of Saturated Clays.* International Journal of Geomechanics, 2016. **17**(3): p.
578   04016068.

579 35. Parkhurst, D.L. and C. Appelo, *User's guide to PHREEQC (Version 2): A computer*
580   *program for speciation, batch-reaction, one-dimensional transport, and inverse*
581   *geochemical calculations.* 1999.

582 36. Patel, V.R., D.S. Upadhyay, and R.N. Patel, *Gasification of lignite in a fixed bed*
583   *reactor: Influence of particle size on performance of downdraft gasifier.* Energy, 2014.
584   **78**: p. 323-332.

585 37. Zainal, Z., et al., *Prediction of performance of a downdraft gasifier using equilibrium*
586   *modeling for different biomass materials.* Energy conversion and management, 2001.
587   **42**(12): p. 1499-1515.

588 38. Perry, R.H., D.W. Green, and J.O. Maloney, *Perry's Chemical Engineer's Handbook*
589   *Chemical Engineer's Handbook.* 1984: McGraw-Hill.

590 39. JANAF Thermochemical Tables, *Stull, DR and Prophet, H.* National Standard
591   Reference Data Series, National Bureau of Standards, Washington, DC, 1971.

592 40. Seetharam, S., H. Thomas, and P.J. Cleall, *Coupled*
593   *thermo/hydro/chemical/mechanical model for unsaturated soils—Numerical algorithm.*
594   International Journal for Numerical Methods in Engineering, 2007. **70**(12): p. 1480-
595   1511.

596 41. Sedighi, M., et al., *Geochemical modelling of hydrogen gas migration in an unsaturated*
597   *bentonite buffer.* Geological Society, London, Special Publications, 2014. **415**: p.
598   SP415. 12.

599 42. Fredlund, D.G., H. Rahardjo, and H. Rahardjo, *Soil mechanics for unsaturated soils.*
600   1993: John Wiley & Sons.

601 43. Thomas, H., et al., *On the development of a model of the thermo-mechanical-hydraulic*
602   *behaviour of unsaturated soils.* Engineering Geology, 1996. **41**(1-4): p. 197-218.

603 44. Thomas, H., Y. He, and C. Onofrei, *An examination of the validation of a model of the*
604   *hydro/thermo/mechanical behaviour of engineered clay barriers.* International Journal
605   for Numerical and Analytical Methods in Geomechanics, 1998. **22**(1): p. 49-71.

606 45. Chen, M., et al., *Dual porosity modelling of the coupled mechanical response of coal*
607   *to gas flow and adsorption.* International Journal of Coal Geology, 2019. **205**: p. 115-
608   125.

609 46. Camp, D.W. and J.A. White, *Underground coal gasification: An overview of*
610   *groundwater contamination hazards and mitigation strategies.* 2015, Lawrence
611   Livermore National Lab.(LLNL), Livermore, CA (United States).

612 47. Hartley, A., *A depositional model for the Mid-Westphalian A to late Westphalian B Coal*
613   *Measures of South Wales.* Journal of the Geological Society, 1993. **150**(6): p. 1121-
614   1136.

615 48. Sadasivam, S., et al., *Baseline geochemical study of the Aberpergwm mining site in*
616   *the South Wales Coalfield.* Journal of Geochemical Exploration, In press.

617 49. Durucan, S., et al., *Two phase relative permeability of gas and water in coal for*
618   *enhanced coalbed methane recovery and CO2 storage.* Energy Procedia, 2013. **37**: p.
619   6730-6737.

620 50. William, E. and D. Airey. *Influence of stress level on the highly compacted shales in*
621   *the Sydney Basin.* in *PROCEEDINGS OF THE INTERNATIONAL CONFERENCE ON*
622   *SOIL MECHANICS AND GEOTECHNICAL ENGINEERING.* 2005. AA BALKEMA
623   PUBLISHERS.

624 51. Van Genuchten, M.T., *A closed-form equation for predicting the hydraulic conductivity*
625   *of unsaturated soils 1.* Soil science society of America journal, 1980. **44**(5): p. 892-
626   898.

627 52. Gensterblum, Y., et al., *High-pressure CH4 and CO2 sorption isotherms as a function*
628   *of coal maturity and the influence of moisture.* International Journal of Coal Geology,
629   2013. **118**: p. 45-57.

630 53. Duan, S., et al., *Adsorption equilibrium of CO2 and CH4 and their mixture on sichuan*
631   *basin shale.* Energy & Fuels, 2016. **30**(3): p. 2248-2256.

632 54. Zagorščak, R., *An investigation of coupled processes in coal in response to high*
633   *pressure gas injection.* 2017, Ph. D. thesis, Cardiff University, Wales, UK.

634 55. Iscan, A. and M. Kok, *Porosity and permeability determinations in sandstone and*
635   *limestone rocks using thin section analysis approach.* Energy Sources, Part A:
636   Recovery, Utilization, and Environmental Effects, 2009. **31**(7): p. 568-575.

637 56. Rodrigues, C. and M.L. De Sousa, *The measurement of coal porosity with different*
638   *gases.* International Journal of Coal Geology, 2002. **48**(3-4): p. 245-251.

639 57. Yang, Y.a.A., A.C., *A permeability–porosity relationship for mudstones.* Marine and
640   Petroleum Geology, 2010. **27**(8): p. 1692-1697.

641 58. Akinlotan, O., *Porosity and permeability of the English (Lower Cretaceous)*
642   *sandstones.* Proceedings of the Geologists' Association, 2016. **127**(6): p. 681-690.

643 59. Li, H., G. Guo, and N. Zheng, *High-temperature effects of the surrounding rocks*
644   *around the combustion space area in SMFM-CRIP—A case study in China.* Energy
645   Sources, Part A: Recovery, Utilization, and Environmental Effects, 2018. **40**(17): p.
646   2021-2036.

647 60. Tang, F., et al., *Thermophysical properties of coal measure strata under high*
648   *temperature.* Environmental Earth Sciences, 2015. **73**(10): p. 6009-6018.

649 61. Kosowska-Golachowska, M., W. Gajewski, and T. Musiał, *Determination of the*
650   *effective thermal conductivity of solid fuels by the laser flash method.* Archives of
651   thermodynamics, 2014. **35**(3): p. 3-16.

652 62. Fujii, T., et al., *Evaluation of CO2 sorption capacity of rocks using a gravimetric method*
653   *for CO2 geological sequestration.* Energy Procedia, 2009. **1**(1): p. 3723-3730.

654 63. Bashir, H., *Methane adsorption into sandstones and its role in gas recovery from*
655   *depleted reservoirs.* 2018, University of Salford.

656 64. Nazaroff, W.W. and R.G. Sextro, *Technique for measuring the indoor radon-222*
657   *source potential of soil.* Environmental science & technology, 1989. **23**(4): p. 451-458.

658 65. Busch, A. and Y. Gensterblum, *CBM and CO2-ECBM related sorption processes in*
659   *coal: a review.* International Journal of Coal Geology, 2011. **87**(2): p. 49-71.

660 66. Day, S., et al., *Swelling of coals by supercritical gases and its relationship to sorption.*
661   Energy & Fuels, 2010. **24**(4): p. 2777-2783.

662